Atmos. Meas. Tech. Discuss., 8, 5735–5768, 2015
www.atmos-meas-tech-discuss.net/8/5735/2015/
doi:10.5194/amtd-8-5735-2015

Atmospheric Measurement Techniques Discussions

Characterization of trace metals with the SP-AMS: detection and quantification

S. Carbone[1,*], T. Onasch[2], S. Saarikoski[1], H. Timonen[1], K. Saarnio[1], D. Sueper[2,3], T. Rönkkö[4], L. Pirjola[5,6], D. Worsnop[1,2,5], and R. Hillamo[1]

[1]Atmospheric Composition Research, Finnish Meteorological Institute, P.O. Box 503, 00101 Helsinki, Finland
[2]Aerodyne Research, Inc. 45 Manning Road, 01821-3976, Billerica, MA, USA
[3]Cooperative Institute for Research In Environmental Sciences, University of Colorado, 80303, Boulder, CO, USA
[4]Tampere University of Technology, Department of Physics, Tampere, Finland
[5]Department of Physics, University of Helsinki, P.O. Box 64, 00014, Helsinki, Finland
[6]Metropolia University of Applied Sciences, P.O. Box 4021, Helsinki, Finland
[*]now at: Department of Applied Physics, University of São Paulo, São Paulo, Brazil

Received: 25 March 2015 – Accepted: 14 May 2015 – Published: 11 June 2015

Correspondence to: S. Carbone (carbone@if.usp.br)

Published by Copernicus Publications on behalf of the European Geosciences Union.

Abstract

A method to detect and quantify mass concentrations of metals by the Aerodyne Soot Particle – Aerosol Mass Spectrometer (SP-AMS) was developed and evaluated in this study. The generation of monodisperse Regal black (RB) test particles with trace amounts of 13 different metals (Na, Al, Ca, V, Cr, Fe, Mn, Ni, Cu, Zn, Rb, Sr and Ba) allowed the determination of the relative ionization efficiency of each metal (RIE_{meas}). The ratio RIE_{theory}/RIE_{meas} presented values larger than the unity for Na, Rb, Ca, Sr and Ba due to the thermal surface ionization (TSI) on the surface of the RB particles. Values closer to the unity were obtained for the transition metals Zn, Cu, V and Cr. Mn, Fe and Ni presented the lowest RIE_{theory}/RIE_{meas} ratio and highest deviation from the unity, which was most likely related to different losses. The RIE_{meas} values obtained in this study were applied to the data of emission measurements in a heavy fuel oil fired heating station. Emission measurements revealed various fragmentation patterns for sulfate, probably because sulfate was mainly in the form of metallic salts (vanadium sulfate, calcium sulfate, iron sulfate and barium sulfate), which were also identified in the high-resolution mass spectrum. The response of the metals to the laser power was also investigated and the results indicated that a minimum current of 0.6 A was needed in the laser in order to vaporize the metals and the rBC. Isotopic pattern of metals was resolved from high-resolution mass spectra and the mass size distribution information of each individual ion was obtained using the high-resolution particle time-of-flight (HR-PToF).

1 Introduction

Trace metals are found in atmospheric aerosol particles and can be originated e.g. from various combustion processes, vehicular emissions, resuspended soil dust, sea-salt and industrial sources (Pacyna, 1998; Allen et al., 2001; Gao et al., 2002; Mbengue et al., 2014). They are frequently linked to adverse health effects, for instance,

AMTD
8, 5735–5768, 2015

chromium, manganese and nickel are among the hazardous air pollutants listed by EPA (EPA 2008). There are several applications where the detection and quantification of the trace metals are desirable. For example, trace elements have been used as tracers for certain emission sources, potassium for biomass burning, vanadium and nickel for petrochemical plants and/or fuel-oil combustion, iron, chromium, manganese, zinc and cadmium for steelwork and smelter emissions (Querol et al., 2007; Mbengue et al., 2014). Moreover, in controlled engine emission experiments the detection of trace elements is useful in order to evaluate the engine performance.

Several offline methods (e.g. X-ray Fluorescence (XRF), Proton-induced X-ray emission (PIXE), inductively coupled plasma mass spectrometer (ICP-MS)) have been previously used to determine trace metal concentrations in aerosol samples (Lough et al., 2005; Querol et al., 2007; Moffet et al., 2008). However, due to low concentrations in ambient aerosol, long sampling times (typically 24–72 h) have been necessary for offline trace metal analysis hindering the investigation of short plumes or diurnal cycles. In that sense, online methods will provide clear improvement in trace metal analysis.

The Aerosol Time-of-Flight Mass Spectrometer (ATOFMS) is one example of an online method, which can detect trace elements in aerosol particles (Prather et al., 1994; Liu et al., 1997). However, the limited particle size range and detection efficiency of this instrument (0.3 % for 95 nm and 44.5 % for 290 nm particles, Su et al., 2004) resulted in a significant constraint for the mass quantification process. The design of the Aerodyne High-Resolution Time-of-Flight Aerosol Mass Spectrometer (AMS) allows quantitative analysis of various chemical species, and was used by Salcedo et al. (2012) to identify and quantify the trace elements copper, zinc, arsenic, selenium, tin and antimony in real time in Mexico City. Additional metals could not be detected due to the limitation of the maximum temperature reached by the vaporizer, typically 600 °C. Onasch et al. (2012) equipped the AMS with a laser vaporizer (Soot Particle – Aerosol Mass Spectrometer, SP-AMS), which allowed refractory material such as soot to be vaporized and measured. Cross et al. (2012) measured with the SP-AMS the trace elements in emissions of a marine engine using the signal of calcium, zinc, magnesium and

AMTD
8, 5735–5768, 2015

phosphorous. Although those trace elements were identified, their mass quantification was not accomplished.

The purpose of this study is to develop a method for quantification of trace metals content in aerosol by using the SP-AMS. The properties of 13 different trace metals (Na, Al, Ca, V, Cr, Fe, Mn, Ni, Cu, Zn, Rb, Sr and Ba) were investigated in a controlled laboratory experiment in order to obtain their theoretical and measured relative ionization efficiencies. The results from the laboratory tests were applied to study fine particles in emissions of a heavy fuel oil fired heating station.

2 Experimental

2.1 Instrumentation

2.1.1 Soot-Particle Aerosol Mass Spectrometer (SP-AMS)

The online chemical composition of submicron particles was measured by using a Soot-Particle Aerosol Mass Spectrometer (Aerodyne Research Inc., USA; Onasch et al., 2012). SP-AMS is a combination of two well-characterized instruments: the Aerodyne high resolution time-of-flight aerosol mass spectrometer (HR-ToF-AMS; Aerodyne Research Inc. MA, USA; DeCarlo et al., 2006) and the single particle soot photometer (SP2, Droplet Measurement Technologies, CO, USA; Stephens et al., 2003). In the HR-ToF-AMS an aerodynamic lens is used to form a narrow beam of particles that is transmitted into the detection chamber, where aerosol components are flash-vaporized upon impact on a hot tungsten surface (600 °C) under high vacuum (Jayne et al., 2000). Only non-refractory species are vaporized at this temperature. The vaporized compounds are subsequently ionized using electron impact ionization (70 eV) and guided to the time-of flight chamber. In the SP-AMS an intracavity Nd:YAG laser vaporizer (1064 nm), based on the design used in the SP2 instrument, was incorporated into the HR-ToF-AMS. The addition of laser enabled to vaporize refractory particles, specif-

AMTD
8, 5735–5768, 2015

ically laser-light absorbing refractory black carbon (rBC). The laser vaporizer does not interfere with the standard tungsten vaporizer used in the HR-ToF-AMS instrument or generate chemical ions. Therefore, the SP-AMS instrument can be operated with the laser vaporizer alone, with both the laser and tungsten vaporizers, or just with the tungsten vaporizer. When operated with both vaporizers, the laser is modulated on and off in order to measure rBC and associated less refractory particulate material in addition to the standard AMS non-refractory species (sulfate, nitrate, ammonium, chloride, organics). In this study, the SP-AMS had both the tungsten and the laser vaporizer operating at the same time. The time resolution for the SP-AMS was set to 30 s. Half of the time the AMS measured PToF (size distribution) and the other half mass spectra (mass concentration without particle size information). During this experiment the collection efficiency was set to the unity value (CE = 1).

2.1.2 Other instruments

In the laboratory experiment other instruments were deployed. The Constant Output Atomizer (TSI model 3076) was operated at constant pressure (~ 2 bar). The Differential Mobility Analyzer (DMA, TSI model 3080) operated at 10 L min^{-1} sheath air and the Condensation Particle Counter (CPC, TSI model 3772) at 1 L min^{-1} of aerosol. Also the silica gel drier TOPAS (length 25 cm) and a sonic probe (ultrasonic cleaner Branson 200) were used in order to dry the aerosol particles and promote the dispersion of the components, respectively.

In the field a comprehensive experimental setup was used. More detailed information on the setup is given in Frey et al. (2014). Briefly, the exhaust from the oil burner was first diluted using filtered air and then studied for particles with online instrumentation and using sample collection for subsequent chemical analysis. Dilution ratio was calculated on the basis of CO_2 concentration in raw flue gas and in the diluted sampled air. The offline methods included the nano-MOUDI cascade impactor (Model 125B) allowing size-segregated sampling of particles in the size range of 10 nm–10 µm. For metals,

AMTD
8, 5735–5768, 2015

the inductively coupled plasma-mass spectrometry was used to determine trace metal concentrations in nano-MOUDI substrates.

2.2 Standards and solutions

Standard solutions of 13 different metals (Na, Al, Ca, V, Cr, Mn, Fe, Ni, Cu, Zn, Rb, Sr and Ba in 2 % nitric acid, Sigma-Aldrich), Regal black (REGAL 400R pigment black, Cabot Corp.) and deionized water were used to make the solutions for the laboratory experiments. The exact mass concentration of each trace metal standard, as well as the relative atomic mass and isotopic composition are depicted in Table S1.

The standard metal solutions were used to make one solution, called hereafter as metal solution, containing 1×10^{-6} kg of each metal and filled to 0.1 L with deionized water (concentration of 1×10^{-5} kg L^{-1}). Of the metal solution 1×10^{-3} L was added to the Regal black solution per time (from zero to 8), as a result the amount of each metal varied between zero and 8×10^{-8} kg. The Regal black solution consisted of 2.4×10^{-5} kg of Regal black (RB) in 0.2 L of deionized water (concentration of 1.2×10^{-4} kg L^{-1}) and was kept constant throughout the study, i.e. no Regal black was added or removed from the original Regal black solution. The concentration of each metal was evaluated in the Regal black solution, before the addition of any metal, to verify possible contamination. From the metals evaluated in this study, only Na could be identified in concentration lower than 0.1 %. The others were not identified likely because they were below the limit of detection indicating low background concentration of metals in the original Regal black solution. The Regal black solution was used as a carrier for the metals and as a light absorbing material because the laser vaporizer employed by the SP-AMS is optimal for carbon clusters vaporization (1064 nm). Thus, Regal black was needed in the solution for the metals to be vaporized. The Regal black signal measured by the SP-AMS was called rBC (sum of the C1 to C5 carbon clusters).

One important point concerning the metals solution was that in terms of stoichiometry there was an excess of nitric acid in comparison to the metals, which means that the metals were most likely in the form of metallic ions.

AMTD
8, 5735–5768, 2015

2.3 The method to measure metal concentrations

The key point for determining the quantitative metal mass concentrations with the SP-AMS is to obtain the value of the relative ionization efficiency (RIE) of each metal. Therefore, RIE of each metal measured by the SP-AMS (RIE_{meas}) was estimated by generating Regal black particles with trace amounts of metals and measuring their number concentration by using a CPC. Particle number concentrations were then converted to corresponding mass concentrations and those values were compared with the RIE values obtained from the literature (RIE_{theory}). When the ratio between RIE_{meas}/RIE_{theory} approaches the unity, the method was assumed to represent well the theory and the method was most likely suitable for quantitative metal detection. The following sections describe the generation of aerosol particles in the laboratory and the estimation of the RIE values (RIE_{meas} and RIE_{theory}).

2.3.1 Aerosol particle generation

Polydisperse submicron aerosol particles were generated by the atomizer from different solutions containing Regal black, water, and trace metals. The sonic probe was used to provide constant dispersion of the components (Regal black and metals) in the solvent (water). After the atomizer particles were passed through the silica gel drier and directed into the DMA. The DMA generated monodisperse (300 nm, mobility diameter) aerosol, which was split between the CPC ($1\,L\,min^{-1}$) and the SP-AMS ($0.1\,L\,min^{-1}$). A schematic diagram of the setup used is shown in the Supplement (Fig. S1).

2.3.2 Relative ionization efficiency estimations and mass calculation

The RIE value of the specie s (relative to nitrate, RIE_s) is required in order to convert the signal of a specific ion measured by the SP-AMS (Hz) into mass concentration ($\mu g\,m^{-3}$) (Eq. 2 in Onasch et al., 2012). The values of the ionization efficiency for each specie (IE_s) and molar weight (MW_s) are needed (Eqs. 3 and 4 in Onasch et al., 2012), which

AMTD
8, 5735–5768, 2015

are not easily found in the literature. For that reason, Jimenez et al. (2003) proposed that the value of IE_s of an ion or molecule is directly proportional to the electron impact ionization cross section (σ), and the number of electrons in an ion or molecule (Ne) is approximately proportional to its molar weight (MW). The values of σ are available in the literature (Table 2) and Ne can be determined once the ion is known.

In this study, the IE of each ion was obtained relative to rBC (where C_3^+ was used as a surrogate of rBC), instead of nitrate, because the rBC was dominant in mass concentration and the carrier component. Hence, the RIE obtained through the ratio σ_s/Ne_s was called theoretical RIE (RIE_{theory}) and it was calculated as described in Eq. (1), where M represents one metallic ion.

$$RIE_{theory} = \frac{\sigma_M}{Ne_M} \Big/ \frac{\sigma_{rBC}}{Ne_{rBC}} \quad (1)$$

To obtain the values of the RIE of each metal measured by the SP-AMS (here called RIE_{meas}), three assumptions were placed, (a) the ratio between the mass of Regal black and each metal was the same in dry particles as in the atomized solution, (b) all generated aerosol particles contained Regal black and (c) particles generated by the atomizer were approximately spherical. Based on those assumptions, the number concentration of particles measured by the CPC was converted into rBC mass assuming monodisperse particles (300 nm, mobility diameter) with density of Regal black (900 $kg\,m^{-3}$). This was called the *CPC mass method*. Thus, the mass of each metal was calculated as shown in Eq. (2):

$$m_M = Z \times m_{rBC}, \quad (2)$$

where m_M and m_{rBC} represent the mass in $\mu g\,m^{-3}$ of one metal M and rBC, respectively, and Z represents the mass fraction of the metal relative to the Regal black in the solution. For instance, in this experiment Z varied between zero and 0.32 %, as the metal solution was added to the Regal black solution gradually (-8×10^{-3} L). Because of the small fraction of metals relative to Regal black in the solution it is assumed that

AMTD
8, 5735–5768, 2015

the particles were mainly composed of the Regal black and the metals were attached to its surface or interior.

2.3.3 Thermal surface ionization

The surface ionization (SI) takes place when an atom or molecule is ionized due to the interaction with a solid surface, and it is dependent on the work function and temperature of the surface and the energy required by each atom or molecule to be ionized (Todd, 1991). If the surface is heated, that process is also referred as thermal ionization (Todd, 1991). In this study the surface ionization on a heated surface will be called thermal surface ionization (TSI).

The TSI was first reported in the Aerodyne AMS by Allan et al. (2003) with K^+ ions formed at the heated surface ($\sim 600\,^{\circ}C$) of the tungsten vaporizer. In general, this type of ionization is undesirable because it produces ions with different energies associated than the ones produced by the electron-impact (EI) ionization, which may complicate the mass quantification process by the SP-AMS. However, in order to investigate the possibility of TSI a quick experiment was carried out in the laboratory. The tungsten vaporizer was turned off and the ionization current set to zero. Under those conditions an electron ejection from the filament, and therefore the EI ionization was unlikely, and the TSI was dominant. The results obtained in this experiment will be discussed in the results section.

2.4 Field measurements

Field measurements were carried out in an oil-fired heating station in Helsinki, Finland from 12 to 15 December 2011. Besides the SP-AMS, several different instruments measured the emissions from three different boilers that burned different combinations of heavy-fuel oil and light-fuel oil with or without water as an emulsion. Further information concerning the instrument setup and measurements were presented in Happonen et al. (2013) and Frey et al. (2014).

AMTD
8, 5735–5768, 2015

3 Results and discussions

3.1 Results of the method development

3.1.1 Identification of metals with isotopic patterns

The identification of metals was performed by using their exact m/z ratios and by investigating their isotopic patterns. However, the low signal observed for several isotopes, due to their low isotopic composition, prevented the determination of some of the isotopes. Barium was used as an example here, since it had the best signal. For instance the isotopes ^{134}Ba, ^{135}Ba, ^{136}Ba, ^{137}Ba and ^{138}Ba corresponded to 99.79 % of the Ba total mass, where ^{138}Ba itself represented 71.69 % (Watson et al., 2004), Table 1. The isotopic compositions (IC) were evaluated relative to the most abundant isotope (^{138}Ba) and the relative isotopic compositions (RIC) obtained by the SP-AMS were compared to the reference RIC (Watson et al., 2004). The agreement varied from 58 to 96 %, i.e. the ratio between ^{137}Ba and ^{138}Ba measured with the SP-AMS represented 96 % of the reference ratio value (Table 1), while the ratio measured ^{134}Ba to ^{138}Ba represented only 58 % of the reference ratio value. The disagreement for ^{134}Ba was probably due to the low signal of this ion (2.4 % of ^{138}Ba signal and below one Hz). In addition, the signal of the different isotopes showed clear linear variation with the signal of ^{138}Ba, the linear correlations (r^2, Pearson correlation) varied from 0.68 to 0.91, Fig. 1. A complete list of the elements and respective isotopes identified in this study can be found in the Supplement, Table S1.

3.1.2 Size distributions

The size distributions of metals were investigated in order to validate the performance of the particle generation system. Size distributions were calculated by using the algorithm implemented to Squirrel version 1.52 L and Pika version 1.11 L AMS analysis software (Sueper, 2008, http://cires.colorado.edu/jimenez-group/ToFAMSResources/

AMTD
8, 5735–5768, 2015

ToFSoftware/) that allowed to obtain the size distribution information of each individual ion measured by the SP-AMS (hereafter called HR-PToF). The average mass HR-PToF size distributions of ^{51}V, ^{52C}r, $^{88}Sr^{+}$, and rBC are presented in Fig. 2. The signal intensity of the rBC as a function of the size distribution was estimated based on its mass spectrum, which was composed by 27.6 % C_1^+, 15.8 % C_2^+, 44.3 % C_3^+, 3.8 % C_4^+ and 4.8 % C_5^+. The sum of C_1-C_5 represented 96 % of the total rBC signal. The results depicted a clear unimodal size distribution for all the metals and the rBC centered at 230 nm (vacuum aerodynamic diameter, d_{va}) and was assumed to correspond the desired 300 nm mobility diameter. The conversion from mobility diameter to d_{va} has been previously described by DeCarlo et al. (2004) and depends on the density of Regal black and the metals in solution standards.

3.1.3 The effect of the laser power

The response of the metals and rBC to the laser power was also studied. Here, the laser current worked as an indicator for the laser power. Increasing gradually from zero, there was a clear increase in the signal of all the metals and rBC when the current was set to 0.4 A. However, the value of 0.4 A was likely not enough to fully vaporize the rBC (about 60 mW according to Onasch et al., 2012). At that current, most of the metals reached their maximum signal immediately, whereas for rBC current up to 0.6 A was needed to reach its maximum signal. This fact indicated that all the other species were more volatile than rBC that requires about 4000 °C to evaporate. It also suggested that once rBC is present in the particles the vaporization and ionization of the metals were achieved. After this threshold current (0.4 A for metals and 0.6 A for rBC) the increase in current did not increase the signal, and any current below the threshold (0.6 A) is not suitable for vaporization of particles containing rBC and metals. All metals presented close to zero signals (< 1 %) when the laser was operated below 0.4 A, also rBC was below 1 % (Fig. 3). The only exceptions were nitrate and ammonium, which were probably in the form of the ammonium nitrate salt and represented about 10 %

AMTD
8, 5735–5768, 2015

of the rBC signal. This fact suggested the presence of particles without rBC that were vaporized by the tungsten vaporizer.

3.1.4 Thermal surface ionization

In order to study the TSI effect the tungsten vaporizer was turned off and the ionization current set to zero. Under these conditions the ions Cr^+, V^+, Ca^+, Al^+, Sr^+, Ba^+, Na^+ and Rb^+ (here in descendent order of ionization energy) and their respective isotopes were identified in the mass spectrum of the SP-AMS, Fig. S2. Because the tungsten vaporizer was cold (~ 100 °C, heated only by the ionizer) and the rBC concentration was abundant, it is hypothesized that those ions were ionized on the hot surface of the rBC. The presence of such isotopic patterns means that the EI ionization was not the only process responsible for ionization. In fact, in the case of the ions mentioned above, the TSI is very significant in determining the mass concentration. In addition to the eight metals mentioned above, also potassium (K) was present in the mass spectrum (Fig. S2, with same isotopic composition verified by the NIST database $^{41}K/^{39}K = 7\,\%$). Because this metal was not present in the solutions used in this experiment, it was likely originated in the ceramics of the filament or contamination.

Another example of isotope detected with the tungsten vaporizer and ionizer off was the isotope $^{44}Ca^+$ (IC = 2 %) in mass-to-charge ratio 44. The presence of this ion in the mass spectrum under typical instrumental conditions (ionizer and vaporizer on) is very atypical due to the constant interference from the ion CO_2^+, which is present in the same mass-to-charge ratio and EI ionization process.

3.1.5 Relative ionization efficiency of metals

Measured relative ionization efficiency

The signal of each metal measured by the SP-AMS (in Hz) was plotted as a function of the mass obtained by the CPC method (Eq. 2) for all the different concentrations of the

AMTD
8, 5735–5768, 2015

metals solution. The slope from this comparison (α_M) was then divided by the slope obtained from the rBC mass calibration (β_{rBC}), which was performed before the current experiment under the same conditions. The rBC calibration process was performed as described by Onasch et al. (2012). The ratio between the two slopes represented the value of the ionization efficiency of the metal M measured relative to the rBC, Eq. (3) (RIE_{meas}, Fig. 4). The measured signal by the SP-AMS (Hz) as a function of the mass concentration obtained by the CPC ($\mu g\,m^{-3}$) for each individual metal and respective slopes are available in the Supplement (Fig. S3).

$$RIE_{meas} = \frac{\alpha_M}{\beta_{rBC}} \quad (3)$$

Measured vs. theory

The ratio RIE_{meas}/RIE_{theory} enabled the evaluation of the performance of the method suggested in this study (Table 2). Values much larger than the unity were obtained for the alkali Na, Rb, Ca (the isotope ^{42}Ca was used to estimate ^{40}Ca due to interference of Ar at m/z 40) and the alkaline earth metals Sr and Ba. Those metals require lower amount of energy to be ionized and therefore are more susceptible to be surface ionized, as already described in the previous section. Values closer to the unity were obtained to the Al, V, Cr and Zn (C_3 was equal to the unity because it was used as a reference), which indicated that the measured RIE for those metals was similar to the theoretical and the method used here was suitable for them. The transition metals Mn, Fe and Ni presented the lowest ratio and highest deviation from the unity (0.36, 0.47, 0.28). One plausible explanation was the possibility of losses. The losses could have occurred at three stages, (1) losses in the atomizer, where the soot surface area (or volume) was not kept constant per droplet (or mass of metal), (2) formation of side products, such as metallic oxides and (3) losses in the laser vaporizer due to the high temperature required to evaporate certain metals. The laser vaporizer beam in the SP-AMS does not fully overlap the particle beam. That is, the metals that require higher temperatures to evaporate were only vaporized when positioned close to the center of

AMTD
8, 5735–5768, 2015

the laser beam, position where the temperature is the highest (~ 4000 °C). At the borders of the laser beam only metals that required lower temperatures were vaporized.

The determination of the IEs of each metal M relative to rBC ($RIE_{M,\ rBC}$) has an important implication, which is in order to implement those values of RIE_M into the AMS software analysis Pika (Sueper, 2008) it is necessary to convert them into $RIE_{M,\ nitrate}$. The conversion can be achieved by simply multiplying the obtained RIE_M relative to rBC ($RIE_{M,\ rBC}$) by the RIE of rBC relative to nitrate ($RIE_{rBC,\ nitrate}$), as shown in Eq. (4). For example, RIE for V^+ ($RIE_{V,\ rBC}$) obtained in this study was 1.36 (Table 2) and the RIE of rBC (now relative to nitrate, $RIE_{rBC,\ nitrate}$) was 0.25 (Fig. 5), therefore the $RIE_{V,\ nitrate}$ value to be implemented into Pika is 0.34.

$$RIE_{M,\ nitrate} = RIE_{rBC,nitrate} \times RIE_{M,rBC} \quad (4)$$

Another important implication was that the RIE_M will be dependent on the value of the RIE_{rBC}, which means that this value must be known. This value was measured and proposed by Onasch et al. (2012) to be 0.2 ± 0.1 and can be used in the studies where it is not possible to measure it.

3.2 Results of the field application

3.2.1 Measurements in an oil-fired heating station

Field measurements in an oil-fired heating station in Helsinki, Finland were accomplished from 12 to 15 December 2011. The average mass spectrum during one of the operating conditions (mixture of light and heavy fuel oil, and water as emulsion with power of 47 MW) indicated the presence of rBC, organics, sulfate and metals (Na, Mg, K, Ca, V, Cr, Fe, Ni, Cu, Zn, Rb, Sr, Sb, Cd and Ba) in the emissions, shown in Fig. 5. When studied in more detail the HR mass spectra indicated the presence of less typical fragments, such as aluminum silicate (Al_2SiO_5), metallic oxides (fragments ZnO_2, CaO, CrO, FeO) and the metallic salts (fragments $VOSO^+$, $VOSO_2^+$, $CaSO_2^+$, $FeSO_4^+$ and $BaSO_2^+$, Fig. 6). Metals and metallic sulfates present a clear negative mass defect,

AMTD
8, 5735–5768, 2015

shown in Fig. 5. This fact facilitates their identification and quantification. In ambient measurements sulfate is typically found in the form of ammonium sulfate (if neutralized) instead of metallic salts. In this experiment ammonium sulfate formation is unlikely due to the reduced amount of ammonium. The presence of elevated concentrations of sulfate and reduced concentrations of ammonium were confirmed by the SP-AMS and parallel ion chromatography analysis of the filter samples (Frey et al., 2014).

3.2.2 Sulfate fragmentation pattern

Fragmentation in the AMS instruments results from the 70 eV EI ionization process employed, where sulfate main fragments correspond to the ions SO^+, SO_2^+, SO_3^+, HSO_3^+ and $H_2SO_4^+$. It has been observed that in an ambient environment where the sulfate was mainly in the form of ammonium sulfate, the last four fragments as a function of SO^+ presented constant slopes for each AMS instrument (Allan et al., 2004).

In this field study, the slopes of those fragments (SO^+, SO_2^+,SO_3^+, HSO_3^+ and $H_2SO_4^+$) as a function of SO^+ were studied and instead of a constant value different values were obtained, Fig. 7. In the vaporization process, the tungsten and laser vaporizer may transfer different internal energies to the vapors, which may cause different EI fragmentation patterns (Alfarra et al., 2004; Onasch et al., 2012). Because the SP-AMS had both vaporizers embedded (switching the laser on/off) two distinct slopes would be expected for each fragment as a function of SO^+. In this field study at least three distinct slopes were found. For example, the fragment SO_2^+ as a function of the SO^+ presented slopes (α) that ranged from 1.02 to 1.27. Conversely, the slopes of the fragments SO_3^+, HSO_3^+ and $H_2SO_4^+$ as a function of SO^+ presented values that ranged from 0.12 to 0.3, 0.11 to 0.31 and 0.05 to 0.17, respectively (Fig. 7). In practice, the presence of multiple slopes could be an indication of the sulfate aerosol particles in the form of metallic sulfates, as it was illustrated by the Figs. 5 and 6. However, those slope values should not be interpreted as numeric indicators because different instruments could present different values due to intrinsic instrumental characteristics, such as ionizer and vaporizer design and configuration.

AMTD
8, 5735–5768, 2015

For comparison, measurements solely with the tungsten vaporizer were depicted together with the measurements with both vaporizers, Fig. 7. Under very low rBC loads similar slopes were obtained for the different vaporizing techniques, which means that the laser vaporization did not take place. This fact is further discussed in the next section.

3.2.3 Mass concentrations and comparison with ICP-MS

The RIE_M values obtained in this study were implemented to Pika v. 1.11 L and the trace metals concentrations were calculated for the field measurements at the oil-fired heating station with the SP-AMS. Besides the SP-AMS, also samples using a nano-MOUDI cascade impactor (Model 125B) were collected (stages 6–13 corresponding to AMS size range) and analyzed with the inductively coupled plasma-mass spectrometry (ICP-MS) method. Figure 8 illustrates the measurements of the metals Fe (the sum of ^{56}Fe, ^{57}Fe and ^{58}Fe), V (^{51}V) and Ba (the sum of ^{134}Ba, ^{135}Ba, ^{136}Ba, ^{137}Ba and ^{138}Ba) by the SP-AMS in $\mu g\,m^{-3}$ using the values of RIEs obtained in this study (Table 2) averaged into the filter sampling times analyzed with the ICP-MS (in $\mu g\,m^{-3}$). Dilution ratios were not applied on.

The comparison presented better agreement between the two techniques for the periods when rBC concentrations were elevated. Larger disagreement between the two techniques occurred in the periods when rBC was very low. These results suggested that a minimum amount of rBC is needed in order to vaporize and detect the refractory material by the SP-AMS, such as metals. The instrumental sensitivity will be discussed in the next chapter.

In addition, the clear evidence of oxides and metallic salts formation (Figs. 7 and 8) in periods of high rBC loads may lead to an underestimation of the metals by the SP-AMS while the ICP-MS method determines the total metal content in the sample. Moreover, the SP-AMS instrument is limited to measure only soot-containing aerosol particles.

AMTD
8, 5735–5768, 2015

3.2.4 Sensitivity

The presence of rBC in the aerosol particles is essential to detect metals with the SP-AMS. Metals associated with the rBC will be evaporated with the 1064 nm wavelength laser and detected. This fact was verified with the measurements at the heating station, by a clear dependence of the metals (sum of all the metals) on the rBC concentrations, i.e. the larger the rBC, the larger the metals concentration (Fig. 9). The different ratios between metals and rBC during the measurements were likely caused by the different conditions during the combustion (e.g., effective fuel spraying, high temperature, optimal air-to-fuel ratio) and the different combinations of fuels used. For example, during efficient combustion periods, small amounts of soot were observed (Frey et al., 2014).

One method to investigate the sensitivity of the SP-AMS for trace metals is to estimate the limit of detection (LD). LD was calculated by using three times the standard deviation of the metal concentration during a period when filtered air was measured (DeCarlo et al., 2006). The LD values were obtained as an average of two minute measurements in one hour of filtered air sampling during the experiment in the heating station. The LD values for metals varied between 10 (Sr^+) and 117 (Mn^+) ng m^{-3}, Table 2. During the same period the LD of rBC was 13 ng m^{-3}. The latter was approximately 3 times smaller than the value reported by Onasch et al. (2012) probably due to the different averaging time employed (one minute).

Interestingly, at the heating station, concentrations of Fe slightly below the limit of detection of the instrument continued to present a linear dependence on the rBC concentrations (Fig. S4). However, larger scatter and deviation from the linearity was observed when the ratio (between Fe and the rBC concentration) was very small (< 0.1). This fact suggests that the ratio between the metals and the rBC could be important in the detection of small concentrations of metals and that metals concentrations slightly below the limit of detection reported here might still be possible to measure with the SP-AMS. In addition, in our recent, not yet published, study we found that industrial emissions (ore processing) may give high signal from metals even during low rBC. This

AMTD
8, 5735–5768, 2015

is indication that pure metals or metal compounds may absorb effectively laser light at 1064 nm and evaporate. Together with this fact and the already mentioned rBC dependence quantification of metal concentrations on the basis of SP-AMS signal needs more laboratory and field tests.

3.2.5 Detection of metals in ambient particles

Metals associated with rBC in ambient aerosol particles, for example primary emissions from biomass burning and vehicle exhaust, are expected to be measured with the SP-AMS. Measurements in urban environments with this instrument showed the presence of the rBC on the Aitken and accumulation modes (Massoli et al., 2012) related to different sources with different mixing states (Lee et al., 2015). In the case of externally mixed particles, the detection of metals might be more difficult however, not impossible in the case of metals in the particle that also interact with the 1064 nm wavelength laser. On the other hand, aged aerosol particles are often internally mixed, which may facilitate the metals detection. For example in ambient measurement in Helsinki eight metals (Al, V, Fe, Zn, Rb, Sr, Zr and Cd) were detected with the SP-AMS of which three (Sr, Zr and Cd) were detected only with the particle concentrator (Saarikoski et al., 2014).

4 Conclusions

A method for the detection and quantification of the trace elements with the SP-AMS was presented. Quantification was achieved by obtaining the RIE values for 13 different metals relative to rBC. The method consisted of generating monodisperse aerosol particles using standard solutions for trace metals together with rBC, where the latter served as a carrier for the trace metals.

The values of RIE of each measured metal (RIE_{meas}) were compared to the literature RIE values (RIE_{theory}) and revealed similarity for those metals not significantly affected

AMTD
8, 5735–5768, 2015

by the thermal surface ionization. The trace metals Rb, Na, Ba, Sr were thermally surface ionized on the surface of the rBC particles, which enhanced their RIE values, compared to the theoretical values. Cu, Zn, V and Cr presented RIE_{meas}/RIE_{theory} values close to the unity. The RIE_{meas}/RIE_{theory} ratio value for the transition metals Mn, Fe and Ni were lower than the unity likely due to losses.

In addition, the metals presented a negative mass defect in the mass spectrum that seemed to facilitate its identification and detection. However, because in the ambient the metals are often present in low concentrations; their identification may be hampered by interference of other ions with larger signals. Therefore the use of the isotopes/isotopic composition for their quantification may be useful, e.g. ^{40}Ca and ^{42}Ca.

Moreover, in the laboratory experiment size distribution information of each individual metal was achieved using the high resolution particle time-of-flight measurement (HR-PToF) indicating the presence of unimodal particle size distribution, which suggested that the metals were most likely attached to the rBC surface or interior. Trace metals were also investigated as a function of the laser current/power, a minimum current of 0.6 A, approximately 90 mW, was needed to fully vaporize the metals and the rBC.

The RIE values obtained in this study were tested in a fired-oil heating station in Helsinki. The concentrations of the Ba, V and Fe obtained with the SP-AMS were compared with the samples analyzed by the ICP-MS method. The comparison indicated good agreement for large concentrations of rBC (in raw flue gas). Due to often changes in the combustion conditions, it is possible that the agreement between the two techniques only happened during periods when particles were internally mixed. In addition, metallic salts such as vanadium sulfate, calcium sulfate, iron sulfate and barium sulfate were identified in the mass spectrum of the emissions from the heating station. The presence of those salts resulted in a different sulfate fragmentation pattern than ammonium sulfate, the general form of sulfate in neutral ambient atmospheric aerosols.

AMTD
8, 5735–5768, 2015

The Supplement related to this article is available online at doi:10.5194/amtd-8-5735-2015-supplement.

Acknowledgements. The study was financially supported by Helsinki Energy, Ministry of Traffic and Communications, TEKES in the CLEEN/MMEA programme (WP4.5.2), the Graduate School in Physics, Chemistry, Biology and Meteorology of Atmospheric Composition and Climate Change (University of Helsinki) and the Academy of Finland (Grant no. 259016).

References

Alfarra, M. R., Coe, H., Allan, J. D., Bower, K. N., Boudries, H., Canagaratna, M. R., Jimenez, J. L., Jayne, J. T., Garforth, A., Li, S.-M., and Worsnop, D. R.: Characterization of urban and rural organic articulate in the Lower Fraser Valley using two Aerodyne aerosol mass spectrometers, Atmos. Environ., 38, 5745–5758, 2004.

Allan, J. D., Coe, H., Bower, K. N., Williams, P. I., Gallagher, M. W., Alfarra, M. R., Jimenez, J. L., Worsnop, D. R., Jayne, J. T., Canagaratna, M. R., Nemitz, E., and McDonald, A. G.: Quantitative sampling using an Aerodyne Aerosol Mass Spectrometer. Part 2: Measurements of fine particulate chemical composition in two UK cities, J. Geophys. Res., 108, 4091, doi:10.1029/2002JD002359, 2003.

Allan, J. D., Delia, A. E., Coe, H., Bower, K. N., Alfarra, M. R., Jimenez, J. L., Middlebrook, A. M., Drewnick, F., Onasch, T. B., and Canagaratna, M. R.: A generalised method for the extraction of chemically resolved mass spectra from Aerodyne aerosol mass spectrometer data, J. Aerosol Sci., 35, 909–922, 2004.

Allen, A. G., Nemitz, E., Shia, J. P., Harrison, R. M., and Greenwood, J. C.: Size distributions of trace metals in atmospheric aerosols in the United Kingdom, Atmos. Environ., 35, 4581–4591, 2001.

Cross, E. S., Sappok, A., Fortner, E. C., Hunter, J. F., Jayne, J. T., Brooks, W. A., and Onasch, T. B., Wong, V. W., Trimborn, A., Worsnop, D. R., and Kroll, J. H.: Real-time measuremtns of engine-out trace elements: application of a novel soot particle aerosol mass spectrometer for emissions characterization, J. Eng. Gas Turb. Power, 134, 072801, doi:10.1115/1.4005992, 2012.

AMTD
8, 5735–5768, 2015

DeCarlo, P., Slowik, J. G., Worsnop, D. R., Davidovits, P., and Jimenez, J. L.: Particle morphology and density characterization by combined mobility and aerodynamic diameter measurements. Part 1: Theory, Aerosol Sci. Tech., 38, 1185–1205, 2004.
DeCarlo, P. F., Kimmel, J. R., Trimborn, A., Northway, M. J., Jayne, J. T., Aiken, A. C., Gonin, M., Fuhrer, K., Horvath, T., Docherty, K. S., Worsnop, D. R., and Jimenez, J. L.: Field-deployable, high-resolution, time-of-flight mass spectrometer, Anal. Chem., 78, 8281–8289, 2006.
Environmental Protection Agency: available at: http://www.epa.gov/ttnatw01/188polls.html, last access: 1 June, 2014.
Freund, R. S., Wetzel, R. C., Shul, R., J., and Hayes, T. R.: Cross-section measurements for electron-impact ionization of atoms, Phys. Rev. A., 41, 3575–3595, 1990.
Frey, A. K., Saarnio, K., Lamberg, H., Mylläri, F., Karjalainen, P., Teinilä, K., Carbone, S., Tissari, J., Niemelä, V., Härinen, A., Rautiainen, J., Kytömäki, J., Artaxo, P., Virkkula, A., Pirjola, L., Rönkkö, T., Keskinen, J., Jokiniemi, J., and Hillamo, R.: Optical and chemical characterization of aerosols emitted from coal, heavy and light fuel oil, and small-scale wood combustion, Environ. Sci. Technol., 48, 827–836, 2014.
Fujii, K. and Srivastava, S. K.: A measurement of the electron-impact ionization cross section of sodium, J. Phys. E. At. Mol. Opt. Phys., 28, 559–563, 1995.
Gao, Y., Nelson, E. D., Fielda, M. P., Ding, Q., Lia, H., Sherrella, R. M., Gigliotti, C. L., Van Ryb, D. A., Glenn, T. R., and Eisenreich, S. J.: Characterization of atmospheric trace elements on $PM_{2.5}$ particulate matter over the New York–New Jersey harbor estuary, Atmos. Environ., 36, 1077–1086, 2002.
Happonen, M., Mylläri, F., Karjalainen, P., Frey, A., Saarikoski, S., Carbone, S., Hillamo, R., Pirjola, L.,Häyrinen, A., Kytömaäki, J., Niemi, J. V., Keskinen, J., and Rönkkö, T.: Size distribution, chemical composition and hygroscopicity of fine particles emitted from an oil-fired heating plant, Environ. Sci. Technol., 47, 14468–14475, 2013.
Jayne, J. T., Leard, D. C., Zhang, X., Davidovits, P., Smith, K. A., Kolb, C. E., and Worsnop, D. R.: Development of an aerosol mass spectrometer for size and composition analysis of submicron particles, Aerosp. Sci. Technol., 33, 49–70, 2000.
Jimenez, J. L., J. T. Jayne, Q. Shi, C. E. Kolb, D. R. Worsnop, I. Yourshaw, J. H. Seinfeld, R. C. Flagan, X. Zhang, K. A. Smith, J. Morris, and Davidovits, P.: Ambient aerosol sampling with an aerosol mass spectrometer, J. Geophys. Res.-Atmos., 108, 8425, 2003.
Kim, Y., Migdalek, J., Siegel, W., and Bieron, J.: Electron-impact ionization cross section of rubidium, Phys. Rev. A, 57, 246–255, 1998.

AMTD
8, 5735–5768, 2015

Lee, A. K. Y., Willis, M. D., Healy, R. M., Onasch, T. B., and Abbatt, J. P. D.: Mixing state of carbonaceous aerosol in an urban environment: single particle characterization using the soot particle aerosol mass spectrometer (SP-AMS), Atmos. Chem. Phys., 15, 1823–1841, doi:10.5194/acp-15-1823-2015, 2015.

Liu, D.-Y., Rutherford, D., Kinsey, M., and Prather, K. A.: Real-time monitoring of pyrotechnically derived aerosol particles in the troposphere, Anal. Chem., 69, 1808–1814, 1997.

Lotz, W.: Electron-impact ionization cross-sections for atoms up to Z = 108, Z. Phys., 232–237, 1969.

Lough, G. C., Schauer, J. J., Park, J.-S., Shafer, M. M., Deminter, J. J., and Weinstein, J. P.: Emissions of metals associated with motor vehicle roadways, Environ. Sci. Technol., 39, 826–836, 2005.

Massoli, P., Fortner, E. C., Canagaratna, M. R., Williams, L. R., Zhang, Q., Sun, Y., Schwab, J. J., Trimborn, A., Onasch, T. B., Demerjian, K. L., Kolb, C. E., Worsnop, D. R., and Jayne, J. T.: Pollution gradients and chemical characterization of particulate matter from vehicular traffic near major roadways: results from the 2009 Queens College air quality study in NYC, Aerosol Sci. Tech., 46, 1201–1218, 2012.

Mbengue, S., Alleman, L. Y., and Flament, P.: Size-distributed metallic elements in submicronic and ultrafine atmospheric particles from urban and industrial areas in northern France, Atmos. Environ., 135, 35–47, 2014.

Moffet, R. C., Desyaterik, Y., Hopkins, R. J., Tivanski, A. V., Gilles, M. K., Wang, Y., Shutthanandan, V., Molina, L. T., Abraham, R. G., Johnson, K. S., Mugica, V., Molina, M. J., Laskin, A., and Prather, K. A.: Characterization of aerosols containing Zn, Pb and Cl from an industrial region of Mexico City, Environ. Sci. Technol., 42, 7091–7097, 2008.

Naghma, R. and Antony, B.: Electron impact ionization cross-section of C_2, C_3, Si_2, Si_3, SiC and Si_2C, Mol. Phys., 111, 269–275, 2013.

Onasch, T. B., Trimborn, A., Fortner, E. C., Jayne, J. T., Kok, G. L., Williams, L. R., Davidovits, P., and Worsnop, D. R.: Soot particle aerosol mass spectrometer: development, validation, and initial application, Aerosol Sci. Tech., 46, 804–817, 2012.

Pacyna, J. M.: Source inventories for atmospheric trace metals, in: Atmospheric Particles, IUPAC Series on Analytical and Physical Chemistry of Environmental Systems, edited by: Harrison, R. M. and van Grieken, R. E., Wiley, Chichester, UK, 5, 385–423, 1998.

Prather, K. A. and Nordmeyer, T., Salt, K.: Real-time characterization of individual aerosol particles using time-of-flight mass spectrometry, Anal. Chem., 66, 1403–1407, 1994.

AMTD
8, 5735–5768, 2015

Querol, X., Viana, M., Alastuey, A., Amato, F., Moreno, T., Castillo, S., Pey, P., de la Rosa, J., Sánchez de la Campa, A., Artinano, B., Salvador, P., Garcia Dos Santos, S., Fernandez-Patier, R., Moreno-Grau, S., Negral, L., Minguillon, M. C., Monfort, E., Gil, J. I., Inza, A., Ortega, L. A., Santamaria, J. M., and Zabalza, J.: Source origin of trace elements in PM from regional background, urban and industrial sites of Spain, Atmos. Environ., 41, 7219–7231, 2007.

Saarikoski, S., Carbone, S., Cubison, M. J., Hillamo, R., Keronen, P., Sioutas, C., Worsnop, D. R., and Jimenez, J. L.: Evaluation of the performance of a particle concentrator for online instrumentation, Atmos. Meas. Tech., 7, 2121–2135, doi:10.5194/amt-7-2121-2014, 2014.

Salcedo, D., Laskin, A., Shutthanandan, V., and Jimenez, J.: Feasibility of the detection of trace elements in particulate matter using online high-resolution aerosol mass spectrometry, Aeros. Sci. Technol., 46, 1187–1200, 2012.

Stephens, M., Turner, N., and Sandberg, J.: Particle identification by laser-induced incandescence in a solid-state laser cavity, Appl. Optics, 42, 3726–3736, 2003.

Su, Y., Sipin, M. F., Furutani, H., and Prather, K. A.: Development and characterization of an aerosol time-of-flight mass spectrometer with increased detection efficiency, Anal. Chem., 76, 712–719, 2004.

Sueper, D.: ToF-AMS High Resolution Analysis Software – Pika, available at: http://cires.colorado.edu/jimenez-group/wiki/index.php/ToF-AMS (last access: 1 June 2014), Analysis Software, 2008.

Todd, J. F. J.: Recommendations for nomenclature and symbolism for mass spectroscopy, Pure Appl. Chem., 63, 1541–1566, 1991.

Vainshtein, L. A., Ochkur, V. I., Rakhovskii, V. I., and Stepanov, A. M.: Absolute values of electron impact ionization cross sections for magnesium, calcium, strontium and barium, Sov. Phys. JetP.-USSR, 61, 511–519, 1972.

Watson, P. R., Van Hove, M. A., and Hermann, K.: NIST Surface Structure Database – Ver. 5.0 National Institute of Standards and Technology, Gaithersburg, MD, 2004.

AMTD
8, 5735–5768, 2015

Table 1. Isotopic composition (IC) and relative isotopic composition (RIC) according to NIST database and measured with the SP-AMS.

Element	IC (%) *	RIC *	Measured RIC
^{138}Ba	71.69	1.00	1.00
^{137}Ba	11.23	6.38	6.18
^{136}Ba	7.85	9.12	8.08
^{135}Ba	6.59	10.87	10.22
^{134}Ba	2.41	29.66	17.24

* Watson et al. (2004)

AMTD
8, 5735–5768, 2015

Table 2. Metallic ions evaluated in the laboratory experiment, electron impact cross section (σ), theory relative ionization efficiency (RIE_T), measured relative ionization efficiency (RIE_M), relative ionization efficiency ratio (RIE_T/RIE_M) and limit of detection.

Ion	σ (A^2) (70 eV)	RIE_{theory}	RIE_{meas}	RIE_{meas}/RIE_{theory}	LD ($ng\,m^{-3}$)
Na^+	2.01 [a]	0.77	20.30	26.36	51
Al^+	7.82 [b]	2.50	5.02	2.01	30
Ca^+	5.80 [c]	1.17	287.50	245.23	87
V^+	7.20 [d]	1.26	1.36	1.08	26
Cr^+	7.50 [e]	1.25	0.97	0.77	21
Mn^+	6.80 [d]	1.09	0.40	0.36	117
Fe^+	4.38 [b]	0.67	0.32	0.47	87
Ni^+	6.20 [d]	0.88	0.25	0.28	111
Cu^+	3.75 [d]	0.51	0.43	0.83	90
Zn^+	5.60 [d]	0.74	0.73	0.99	n/a
Rb^+	7.20 [e]	0.77	158.47	206.34	10
Sr^+	8.20 [c]	0.85	23.19	27.24	10
Ba^+	10.50 [c]	0.73	21.42	29.23	11
C_3^+	4.43 [f]	1	1	1	13 [g]

[a] Fujii and Srivastava (1995); [b] Freund et al. (1990); [c] Vainshtein et al. (1970); [d] Lotz (1969); [e] Kim et al. (1998); [f] Naghma and Antony (2013); [g] LD value estimated for rBC.

AMTD
8, 5735–5768, 2015

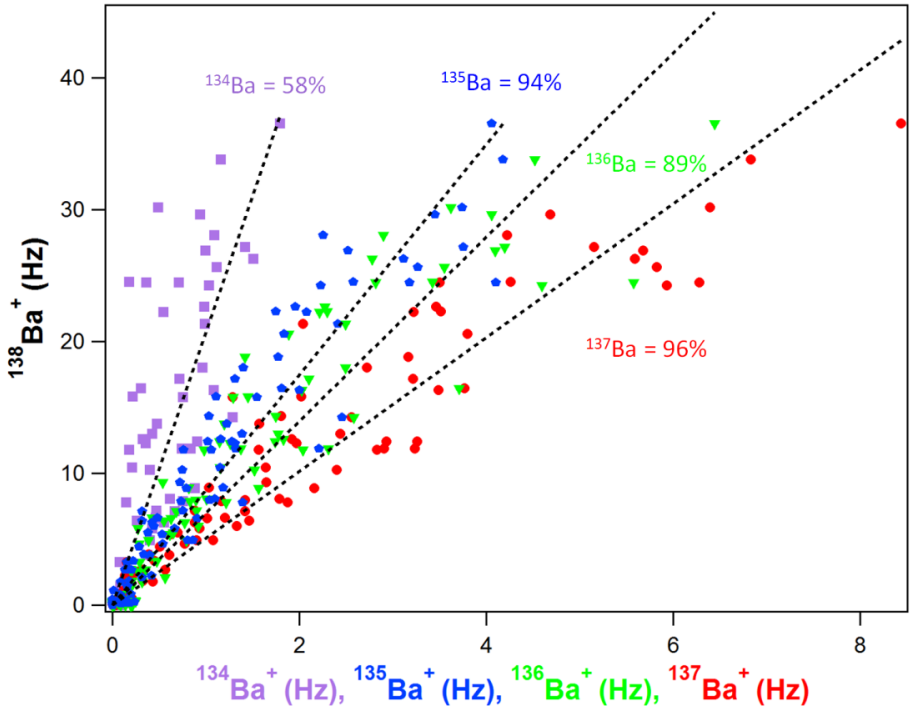

Figure 1. Barium isotopic pattern measured in the laboratory. The percentages correspond to the isotopic compositions relative to the most abundant ($^{138}Ba^{+}$).

AMTD
8, 5735–5768, 2015

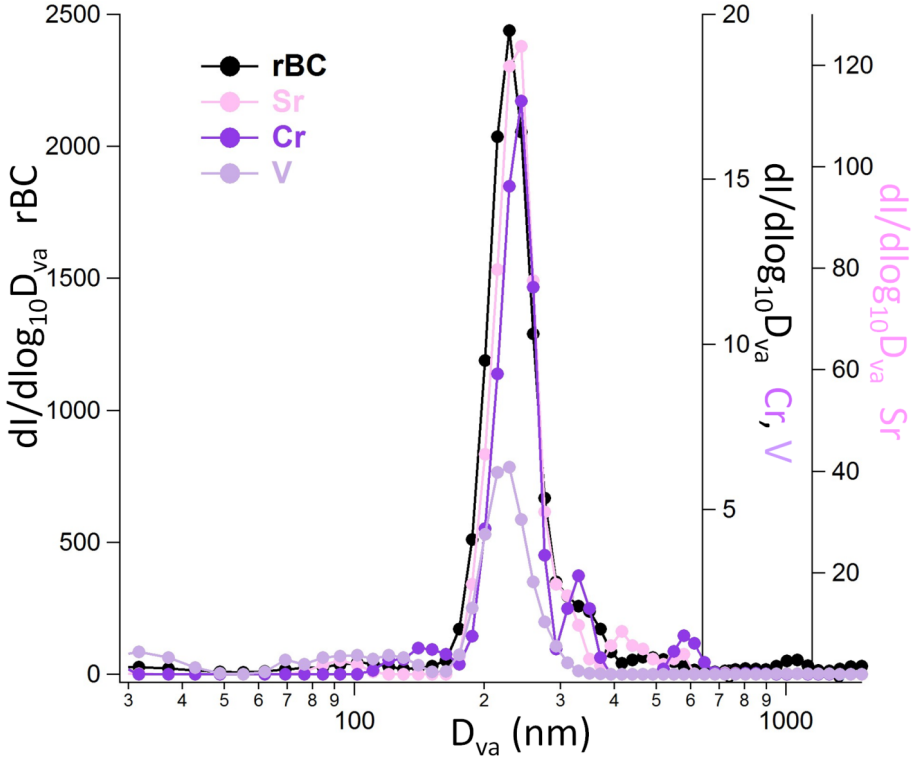

Figure 2. High resolution signal intensity size distributions (HR-PToF) of rBC, V^+, Cr^+ and Sr^+.

AMTD
8, 5735–5768, 2015

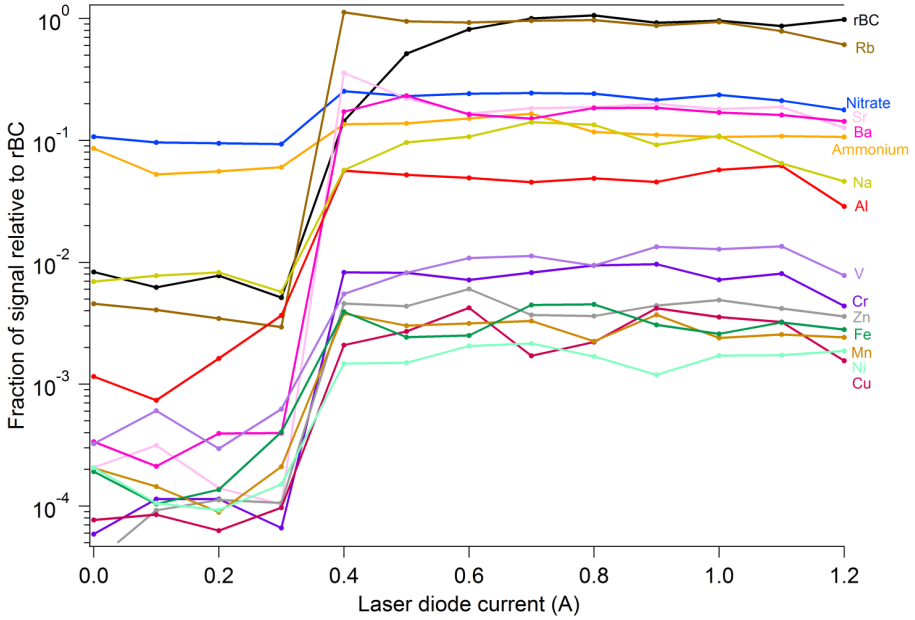

Figure 3. Fraction of metals signal relative to the rBC signal as a function of the laser diode current (LDC) for each metal and rBC.

AMTD
8, 5735–5768, 2015

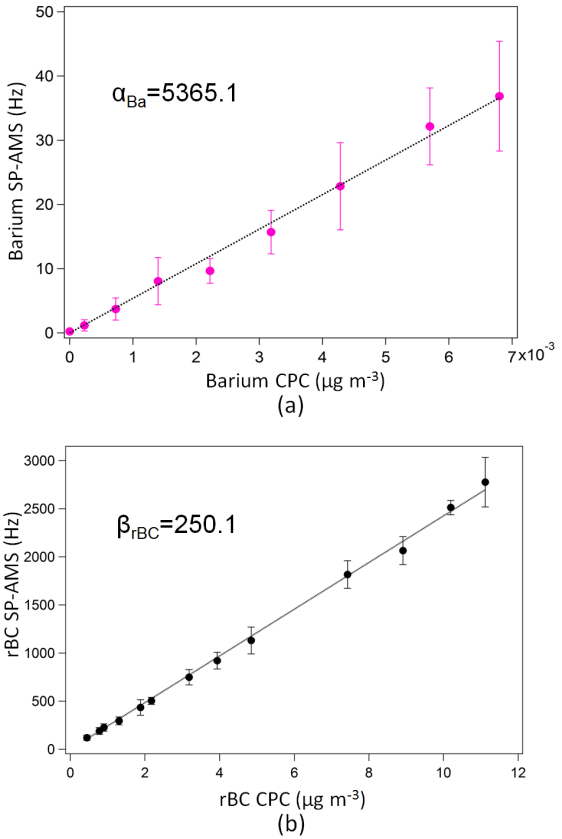

Figure 4. Signal measured by the SP-AMS (Hz) vs. the mass concentration obtained by the CPC (µg m^{-3}) for barium **(a)** and rBC **(b)**.

AMTD
8, 5735–5768, 2015

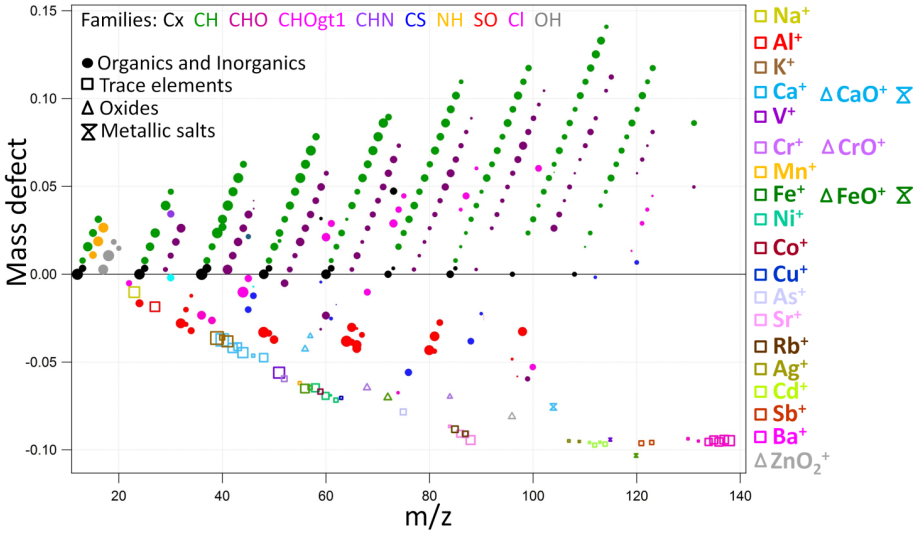

Figure 5. Mass defect (difference between the ions exact mass and its nominal mass) obtained from the emissions of a heavy-fuel oil power plant the size of the marker is proportional to the square root of the signal of each ion. Organic and inorganic ions are represented with circles, metals with squares, oxides with triangles and metallic sulfates with double triangles.

AMTD
8, 5735–5768, 2015

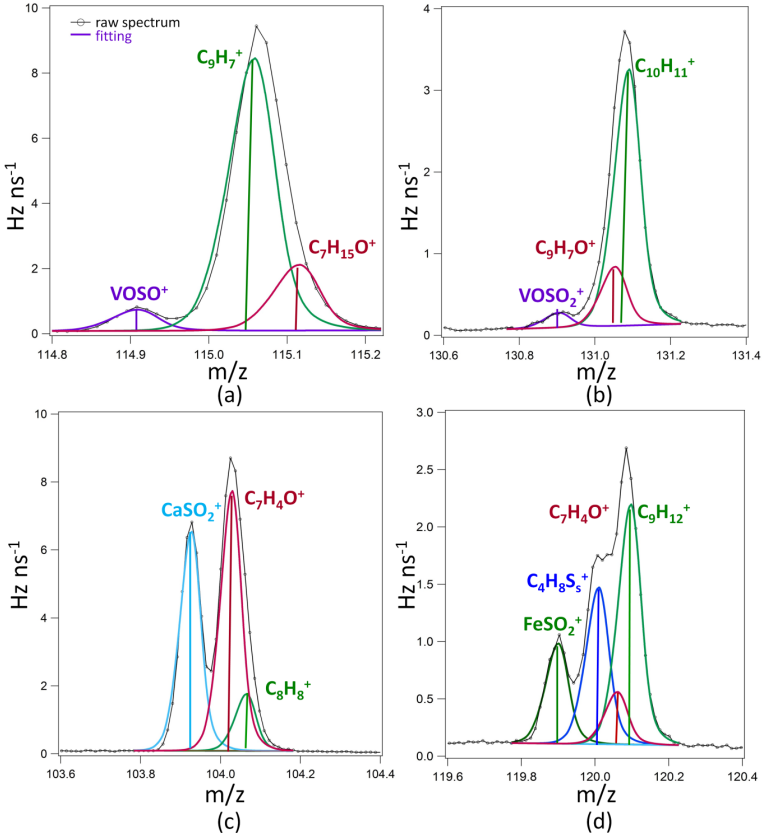

Figure 6. Average high-resolution mass spectra for the *m/z*s 115 **(a)**, 131 **(b)**, 104 **(c)** and 120 **(d)** during field experiment at the heating station.

AMTD
8, 5735–5768, 2015

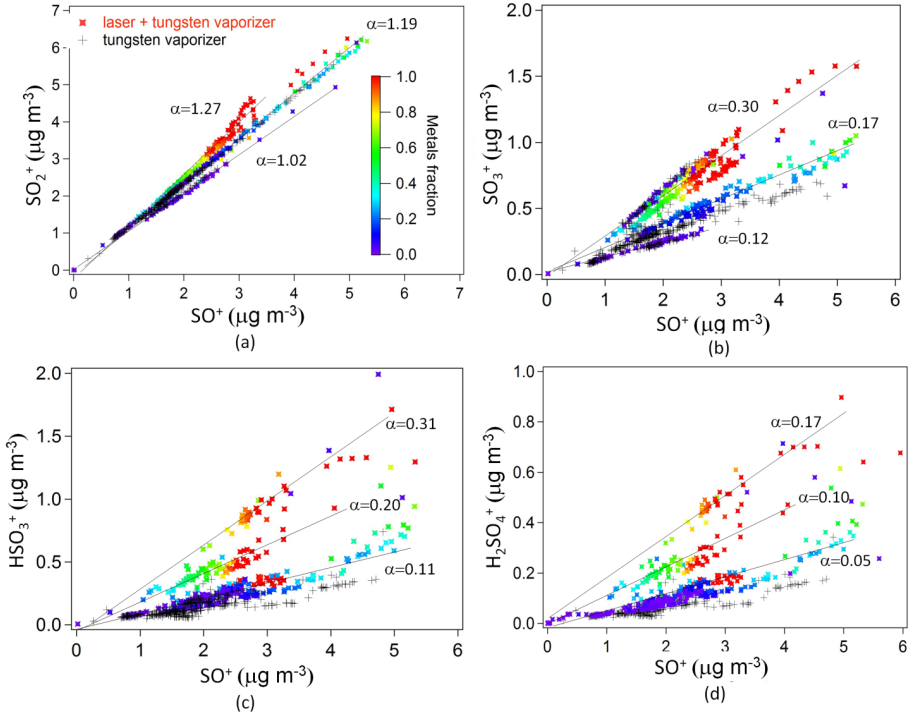

Figure 7. Sulfate fragmentation patterns, SO_2^+ vs. SO^+ **(a)**, SO_3^+ vs. SO^+ **(b)**, HSO_3^+ vs. SO^+ **(c)** and H_2SO^{4+} **(d)** during the field experiment at the heating station. For comparison, the black crosses represent the measurements solely with the tungsten vaporizer.

AMTD
8, 5735–5768, 2015

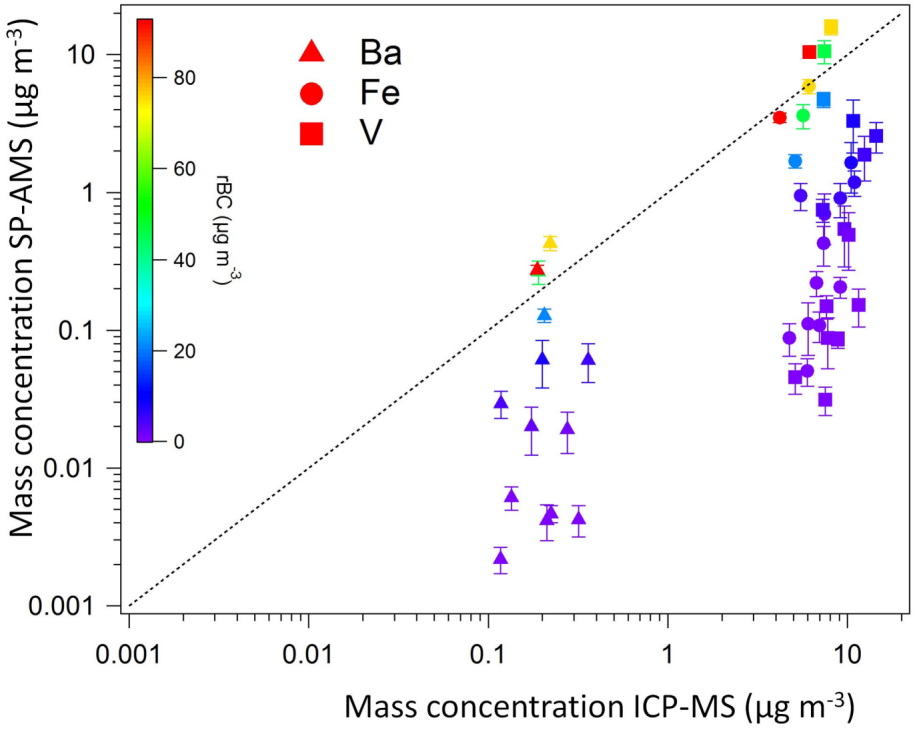

Figure 8. The metals barium, vanadium and iron measured with the SP-AMS vs. the collected with the nano-MOUDI and analyzed with the ICP-MS method (in $\mu g\,m^{-3}$) at the heating station.

AMTD
8, 5735–5768, 2015

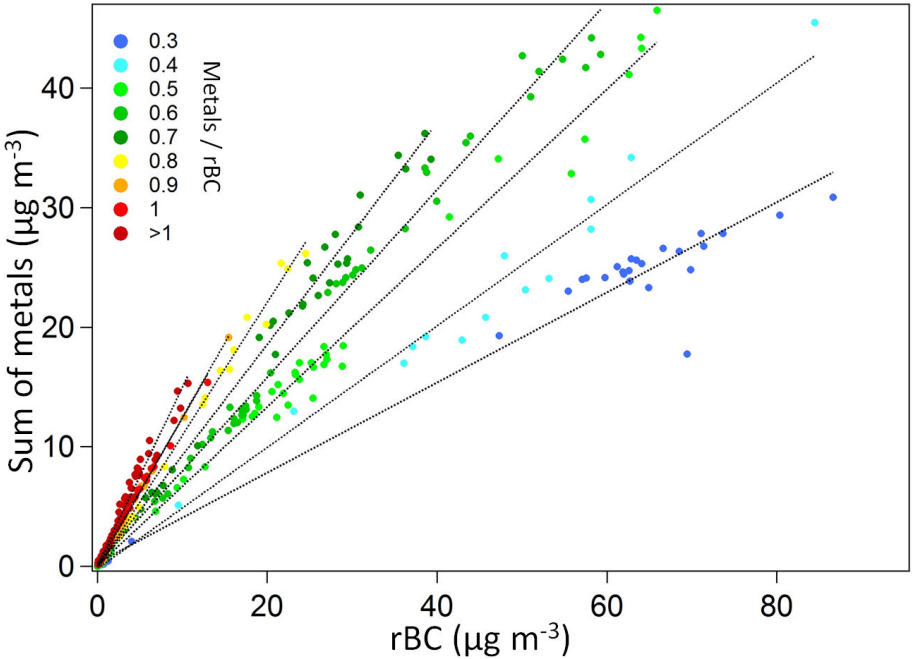

Figure 9. Mass concentration of the sum of all the metals measured at the heating station with the SP-AMS as a function of the rBC concentration.

AMTD
8, 5735–5768, 2015